ORIGINAL RESEARCH

An Analysis Regarding the Association Between Connexins and Colorectal Cancer (CRC) Tumor Microenvironment

Yuan-jie Liu[1,2,]*, Mei Han[1,]*, Jie-pin Li[1–3], Shu-hong Zeng[1,2], Qian-wen Ye[1,2], Zhong-hua Yin[1,2], Shen-lin Liu[1,2], Xi Zou[1,2,4]

[1]Department of Oncology, Affiliated Hospital of Nanjing University of Chinese Medicine, Jiangsu Province Hospital of Chinese Medicine, Nanjing, People's Republic of China; [2]No. 1 Clinical Medical College, Nanjing University of Chinese Medicine, Nanjing, People's Republic of China; [3]Department of Oncology, Zhangjiagang TCM Hospital Affiliated to Nanjing University of Chinese Medicine, Zhangjiagang, People's Republic of China; [4]Jiangsu Collaborative Innovation Center of Traditional Chinese Medicine in Prevention and Treatment of Tumor, Nanjing, People's Republic of China

*These authors contributed equally to this work

Correspondence: Xi Zou; Shen-lin Liu, Email zxvery@126.com; lsljsszyy@126.com

Background: Gap junctions, as one of the major ways to maintain social connections between cells, are now considered as one of the potential regulators of tumor metastasis. However, to date, studies on the relationship between gap junctions and colorectal cancer (CRC) are limited.

Methods: We synthesized connexins-coding gene expression data from public Gene Expression Omnibus (GEO) and The Cancer Genome Atlas (TCGA) databases. Bioinformatics analysis was performed using R software and several database resources such as MEXPRESS database, Gene Set Cancer Analysis (GSCA) database, Human Protein Atlas (HPA) database, Tumor Immune Single Cell Hub (TISCH) database, Search Tool for Retrieval of Gene Interaction Relationships (STRING), and Cytoscape software, etc., to investigate the biological mechanisms that may be involved in connexins. Immunofluorescence and immunohistochemical staining were used to validate the expression and localization of GJA4.

Results: We found that CRC patients can be divided into two connexin clusters and that patients in cluster C1 had shorter survival than in cluster C2. The infiltration of M1 macrophages and NK cells was lower in cluster C1, while the levels of M2 macrophages and immune checkpoints were higher, indicating an immunosuppressed state in cluster C1. In addition, the epithelial–mesenchymal transition (EMT) phenotype was significantly activated in cluster C1. We observed that GJA4 was up-regulated in colorectal cancer tissues, which was related to poor prognosis. It was mainly expressed in fibroblasts, but the expression levels in normal intestinal epithelial cells were low. Finally, we found that GJA4 was associated with M2 macrophages and may be a potential immunosuppressive factor.

Conclusion: We found that there is a significant correlation between abnormal connexins expression and patients' prognosis, and connexins play an important role in stromal-tumor interactions. Connexins, especially GJA4, can help enhance our understanding of tumor microenvironment (TME) and may guide more effective immunotherapeutic strategies.

Keywords: colorectal cancer, gap junction protein alpha 4, cancer-associated fibroblasts, M2 macrophage, bioinformatics

Introduction

Colorectal cancer (CRC) is a tumor of the gastrointestinal system, ranking third in incidence among malignancies and second in lethality among cancers.[1] Its pathogenesis appears to involve multiple factors and steps, including genetics, diet, and lifestyle habits.[2,3] Statistics show that the tumor frequently recurs and metastasizes, spreading especially to the liver, lung, bone, and ovaries, and the five-year survival rate for such patients is approximately 10%.[4,5] Treatment methods for CRC include chemotherapy, surgery, radiotherapy, and molecular-targeted therapy.[6,7] Molecular-targeted therapy for CRC has become a hot topic.[8] The number of molecularly stratified treatment options is increasing, as is the use of biomarkers to guide

prediction and treatment decisions.[9,10] Therefore, the identification of novel markers and targets for treating CRC is necessary for improving the disease prognosis.

Gap junction protein (Connexin) is a four-pathway transmembrane protein involved in the assembly of gap junctions among adjacent cells, thereby facilitating gap junction cell-to-cell communication (GJIC), which allows small molecules and ions to diffuse freely directly from the cytoplasm of neighboring cells without encountering the extracellular environment, resulting in a rapid and coordinated cellular response to internal and external stimuli.[11,12] It is well established that connexins are often considered tumor suppressive due to reduced expression or altered cytoplasmic localization of connexin in primary tumor cells, resulting in GJIC deficiency.[13] However, enhanced expression levels of connexins have also been reported in metastatic lesions, including connexin 43 (Cx43, GJA1) and connexin 26 (Cx26, GJB2), which may function to mediate the promotion of cancer cell migration and adhesion.[14,15] An interesting study in 2016 found that Cx43 localized on fibroblasts could help tumor cells expel excess acid to maintain a favorable ecological environment, which in part reinforces the complex and variable role of connexins.[16] However, to date, studies on the role of connexins in CRC are still very scarce. The present study seeks to fill this lacuna.

In this study, human colorectal cancer specimens were analyzed by immunohistochemistry and immunofluorescence methods. Meanwhile, the potential functions and mechanisms of action of connexins, especially *GJA4*, were initially explored by using bioinformatics software and methods.

Materials and Methods

Reagents
The reagents and antibodies used are listed in the Supplementary Materials (Supplementary Table 1). The concentrations used were based on those used in the previous research or on the manufacturer's recommendations. Experimental procedures are also provided in the Supplementary Material.

Data Sources and Process
The workflow of our research is shown in Supplementary Figure 1. A total of 620 CRC samples, including gene expression profiles and matching clinical data as well as mutation data, were downloaded through the University of California, Santa Cruz (UCSC) browser. The gene expression profiles (FPKM values) of The Cancer Genome Atlas (TCGA) – Colorectal adenocarcinoma (COAD&READ) dataset was processed through R software to transform into Transcripts Per Kilobase million (TPM), which is closer to the microarray data.[17] We then selected the Gene Expression Omnibus (GEO) dataset GSE44861 and GSE10950 for expression and immune cell infiltration analysis.[18–20] Gene expression data were extracted using R software (version 4.1.1), and data matrix was constructed for further analysis.

Establishment of Consistent Clustering Based on Connexins
Consensus clustering algorithm was performed to estimate the number of unsupervised classes in TCGA-COADREAD. The TCGA-COADREAD cases were classified into 2 clusters based on the expression profile of the connexins by "consensusclusterplus" R package. The procedure was repeated 500 times to ensure the stability and reproducibility of the classification. Principal component analysis (PCA) was used to determine the validity of clustering.[21]

Least Absolute Shrinkage and Selection Operator (LASSO) and COX Analysis
The LASSO regression analysis was conducted through the R package "glmnet" to determine the research objective.[22] We conducted the univariate and multivariate Cox regression analysis to access the prognostic values of connexins coding genes. The forest plots representing the P-value, hazard ratio (HRs), and 95% confidence interval (CIs) of all variables were visualized with the "forestplot" R package.

Expression and Survival Analysis
The relationship between RNA sequences and clinical characteristics in TCGA was visualized through the "survival" R package and MEXPRESS database, mainly including Overall Survival (OS), Disease Specific Survival (DSS), Progression Free Interval

(PFI), Progression Free Survival (PFS), Disease Free Survival (DFS), and "T (Tumor)", "N (Node)", "M (Metastasis)" stages.[23] And then, TCGA expression profile and Gene Expression Omnibus (GEO) data were used to assess the differential expression. In addition, the Human Protein Atlas (HPA) and our own immunohistochemical data were used to validate the expression of GJA4 at the protein level.[24]

Ethics Statement and Specimen Collection

The study's protocol was approved by the ethics committee of the Jiangsu Province Hospital of Chinese Medicine, and informed consent was obtained from clinicians and patients (2020NL-107-01). This study complied with the Declaration of Helsinki. The CRC tissue and the surrounding non-tumorous tissue (margin, 5 cm) were collected during surgery from 30 previously treatment-naïve patients with CRC at the Jiangsu Provincial Hospital of Traditional Chinese Medicine. Inclusion criteria: (1) All patients were first pathologically diagnosed with CRC. (2) The diagnosis was referenced to the latest (8th edition) American Joint Committee on Cancer (AJCC) CRC staging system.[25] (3) All patients had complete clinical information. After extraction, tissue specimens were washed with cold phosphate-buffered saline and immediately placed in liquid nitrogen. They were then transferred and stored at −80°C until further examination. Immunohistochemistry (IHC) and Tissue Section Immunofluorescence (IF) staining were performed as previously described.[26,27] The precise details are given in <u>Supplementary Materials</u>.

Enrichment Analysis

The "limma" R package was used to obtain the Differentially Expressed Genes (DEGs) between C1 and C2 clusters and genes co-expressed with *GJA4*. The "clusterProfiler" R package and GSCALite web tool were used to perform the functional enrichment analysis. The protein–protein interaction (PPI) was constructed by STRING online database and visualized by Cytoscape.[28,29] The Cytoscape cytoHubba plugin was used to search for hub genes by degree order, with default parameters being used as parameter settings.[30]

The gene set enrichment analysis (GSEA) was performed through R 4.1.1.[31] The gene set "subset of Gene Ontology (GO)" and "subset of hallmark" were downloaded from the Molecular Signatures Databases and were used as reference gene sets.[32] The False Discovery Rate (FDR) <0.1 was considered to be with statistical significance.

Single Cell Analysis

First, we conducted a single cell analysis based on GSE146771 by Tumor Immune Single Cell Hub (TISCH) database to explore in which cell types *GJA4* may express.[33,34] Then, we downloaded an independent dataset from scTIME Portal, which consists of 1 CRC patient's cells. All samples were imported into Seurat V3 and visualized in UMAP after a standardized quality control process. Next, fibroblasts were distinguished from all cells. The "FindAllMarkers" function (min.pct = 0.25, logfc.threshold= 2, tes.use = "wilcox") was set to find markers for all cell types. 'Dotplot' function was used to plot dot plots, and 'Vlnplot' function was used to plot violin plots.

Genetic Analysis

We conducted the "maftools" package to assess the frequency of mutations in 21 connexins and the Gene Set Cancer Analysis (GSCA) database to calculate the relationship between connexin genetic alterations and expression levels.[35]

Immune Analysis

The CIBERSORT and ssGSEA algorithms were used for the overall assessment of immune infiltration score, and the "estimate" package was used to calculate immune and stromal scores as well as tumor purity.[36,37] The Tumor Immune Estimation Resource (TIMER) database was used for reliable assessment of fibroblast infiltration, and pairwise comparisons were quantified by Spearman's rank correlation, with $P < 0.05$ representing significance. All results were processed using the 'ggplot2' and 'pheatmap' packages in R.[38]

Immunohistochemical and Immunofluorescence Staining

Immunohistochemical and Immunofluorescence Staining and H-sore procedures were performed as described previously.[39,40] A detailed description is shown in Supplementary Materials.

Results

The Genetic Characteristics and Transcriptional Variations of 21 Connexins

We collected the currently available research data on 21 connexins including *GJA1, GJA3, GJA4, GJA5, GJA8, GJA9, GJA10, GJB1, GJB2, GJB3, GJB4, GJB5, GJB6, GJB7, GJC1, GJC2, GJC3, GJD2, GJD3, GJD4*, and *GJE1*. Figure 1A demonstrates that gap junctions among tumor cells are potent regulators of EMT, while little has been reported about the role of gap junctions among non-tumor cells. We first showed various relationships, including interactions, colocalization, and common pathways among connexins (Figure 1B). In CRC tissue, most connexins activated the EMT signaling pathways but inhibited the cell cycle and DNA damage response (Figure 1C). Based on the mRNA data of paired tumor and normal samples present in TCGA-COADREAD, several genes were found to be highly expressed in CRC tissues: *GJA3, GJA4, GJB1, GJB3, GJB4, GJB5, GJB6, GJC3*, and *GJD2* (Figure 1D). We then confirmed that in CRC, genetic variation and DNA methylation were important factors affecting the expression levels of connexins, and that Copy Number Variations (CNVs) and mRNA expression levels were positively correlated, while gene methylation levels and mRNA expression levels were negatively correlated (Figure 1E). In addition, for some of the connexins, these two factors were also able to influence the prognosis of CRC patients (Figure 1F). In the TCGA database, there was a significant co-expression relationship between *GJA1* and *GJA4, GJA5, GJC1*, and *GJD3* ($P < 0.05$, Figure 1G). Out of 544 samples, 96 samples had mutated connexins, with a frequency of 17.65%. Among these 96 samples, *GJA8* had the highest frequency of mutations, mainly missense mutations (Figure 1H). These results strongly suggested that imbalance of connexins can lead to CRC.

Identification and Analysis of Connexin Molecular Clusters of CRC

To identify potential connexin molecular clusters of CRC, we classified 620 CRC cases in the TCGA cohort using consensus clustering analysis. Based on the "ConsensusClusterPlus" R package, all tumor samples were classified into k (k = 2–6) different clusters based on the expression levels of 21 connexins coding genes in GC. According to the results of cluster analysis, we chose k = 2 being the number of clusters, indicating that CRC patients were accurately classified into two clusters (C1 and C2 clusters) (Figure 2A–C). The principal component analysis (PCA) showed that the classification was effective in distinguishing between two clusters of CRC patients (Figure 2D), and Kaplan–Meier survival analyses showed that C1 patients had worse OS, DFS, and PFS relative to C2 patients (Figure 2E–G). In addition, Figure 2H shows the connexins expression profiles based on both clusters and the correlation between the distribution of clinicopathological parameters including T/N/M and pathological stage with the two clusters.

We then analyzed the effect of connexins on the tumor immune microenvironment. We observed that chemokines, interleukins, and alterons had higher expression in cluster C1 than in cluster C2, including CXCL10, CCL7, VEGFB, VEGFC, and TGFBR1 (Figure 2I). In addition, we also found that m6A and ferroptosis-related genes were differentially distributed between cluster C1 and C2 (Supplementary Figure 2A and B). TCGA pathology slide confirmed that there was more infiltration of immune cells in the CRC nests of Cluster C1 patients but less infiltration of immune cells in the CRC tissue of Cluster C2 patients (Figure 2J). Then CIBERSORT algorithm based on TCGA-COADREAD demonstrated that patients in cluster C1 have more M2 macrophage infiltration than those in cluster C2 (Figure 2K) ($P < 0.001$). We finally compared the differences of immune checkpoints (ICPs) between the 2 clusters and most ICPs including *CD274, CTLA4, HAVCR2, LAG3, PDCD1, PDCD1LG2*, and *TIGIT* were significantly higher in C1 than in C2 (Figure 2L) ($P < 0.001$).
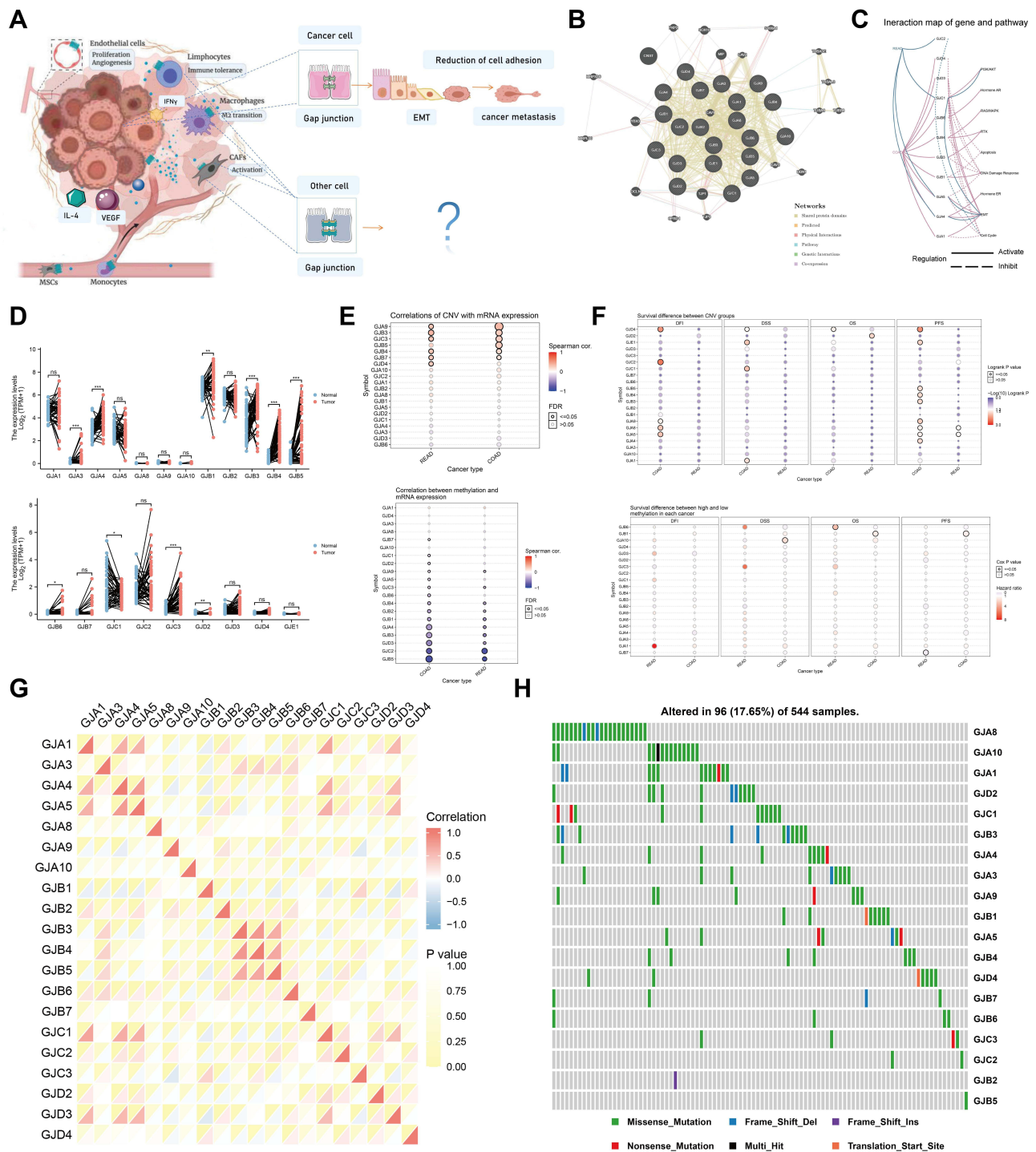
Figure 1 Expression variation of connexins. (**A**) pattern map shows the molecular regulatory mechanism of connexins and their potentially important regulatory role in EMT of tumor/non-tumor cells. (**B**) Connexins with neighboring genes showing physical interactions, co-expression, co-localization, predicted common pathways, genetic interactions, and common protein domains. (**C**) The correlation between the 11 connexins in CRC and important cancer associated signaling pathways. The solid line represents activation and the dashed line represents inhibition. (**D**) Differential expression of connexins between CRC and paired normal tissues. (**E**) Relationship between CNVs, DNA methylation and connexins expression. Red indicates positive correlation; blue indicates negative correlation. The deeper color indicates a larger correlation index. The bubble size indicates the FDR. (**F**) The correlation between CNVs, DNA methylation of the 21 connexins and CRC patients' survival including DFI, DSS, OS, PFS. Red shows a positive correlation and blue shows a negative correlation. The darker color indicates a larger correlation index. Bubble size indicates the FDR. (**G**) Correlation between expression levels of connexins, red represents positive correlation, blue represents negative correlation, and shades of yellow indicates the P values. (**H**) Mutation frequency of 21 connexins in 620 patients with CRC in the TCGA-COADREAD cohort. Each column represents an individual CRC patient. (*P < 0.05, **P < 0.01, ***P < 0.001).
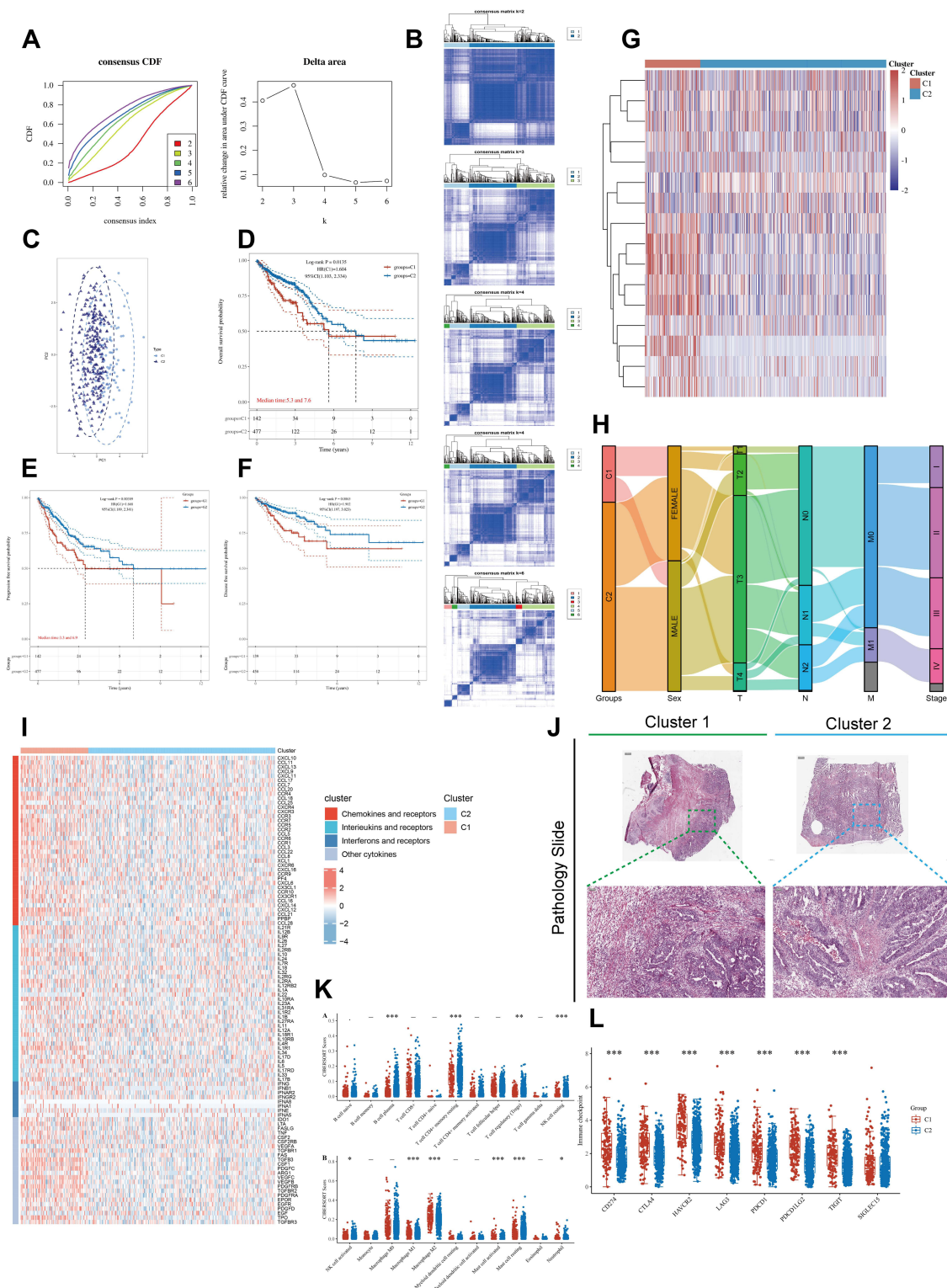**Abbreviation**: NS, not significant.

Figure 2 The landscape of connexins in CRC and the characteristics of two clusters. (**A**) The cumulative distribution function (CDF) curves in consensus cluster analysis. CDF curves of consensus scores by different subtype numbers (k = 2, 3, 4, 5, and 6) were displayed. Relative change in area under the CDF curve for k = 2–6 was also shown. (**B**) The consensus score matrix of all samples when k = 2–6. (**C**) The PCA distribution of TCGA-COADREAD samples by expression profile of connexins. Each point represents a single sample; different colors represent the C1 and C2 clusters respectively. (**D–F**) Survival analysis of (**D**) OS, (**E**) PFS, and (**F**) DFS based on two clusters. (**G**) Expression distribution of 21 connexins between two clusters, connexins with 0 expression in most samples have been removed. (**H**) Distribution of clinical characteristics of two subtypes, including 'tumor-node-metastasis'' (TNM) stages and pathological stage. (**I**) The thermogram shows variations in mRNA expression of chemokines, interleukins, alterons, and other cytokines between two clusters. (**J**) Representative pictures of pathological HE staining of two clusters. (**K–L**) The differences of (**K**) TME infiltrating cells and (**L**) common immune checkpoints between the two connexins phenotypes (Kruskal–Wallis test). (*P < 0.05, **P < 0.01, ***P < 0.001).

Identification of Functional Differences Between Two Clusters

We first identified the 20 genes with the highest mutation frequencies in CRC (Figure 3A) and then compared the differences in mutation frequencies of these 20 genes between the two clusters (Figure 3B). The differences in gene expression between subtypes of connexin and the characteristics of the associated signaling pathways were then explored. We observed that in CRC, especially *GJC1, GJA5, GJA4* showed a 100% level of activation in the EMT signaling pathway, but consistent inhibition of the cell cycle and DNA damage response (Figure 3C). A total of 305 DEGs were screened based on the analysis by CRC gene expression profiles; 276 were up-regulated and 29 were down-regulated in cluster 1 relative to cluster 2 (Figure 3D). Then, all DEGs were used for the assembly of PPI, and based on the degree value from cytoHubba, 10 hub genes including *FN1, DCN, POSTN, COL1A1, THBS2, MMP2, COL1A2, COL3A1, COL5A1* and *BGN* were identified (Figure 3E), all of which have strong activation effect on EMT in CRC (Figure 3F). GSEA showed that EMT, angiogenesis and macrophage activation were significantly activated in the cluster C1 (Figure 3G).

Subsequently, 21 connexins were used for LASSO regression to identify robust markers for follow-up studies. Cross-validation was performed in ten rounds to prevent overfitting (Figure 3H). Sequential Cox regression (both univariate and multivariate) indicated that *GJA3, GJA4, GJB6* were significantly correlated with CRC prognosis (Figure 3I). The calculation results based on two independent datasets (GSE44861 and GSE10950) showed that *GJA4* was overexpressed in CRC tissues (Figure 3J), consistent with the results from TCGA (Figure 1D). Finally, these three genes acting as potential cancer-promoting factors were shown to be significantly highly expressed in cluster C1 (Figure 3K), and all of them, especially *GJA4*, were significantly associated with the degree of immune cell infiltration (Figure 3L).

Clinical Analysis of *GJA4*

The results of the HPA database suggested that GJA4 was significantly highly expressed at the protein level in CRC tissues relative to normal tissues (GJB6 was not included) (Figure 4A and B). Then, the role of *GJA4* in CRC was generally assessed. In cases from MEXPRESS categorized based on different clinical factors, including colon polyps present, lymphatic invasion and sample type, *GJA4* displayed the differences in expression patterns (Figure 4C and D). The results of independent calculations based on TCGA-COADREAD showed that the *GJA4* expression level was correlated with pathologic stage and T stage (Figure 4E). Kaplan–Meier survival curves were then constructed to validate the prognostic value of *GJA4* and the results showed that patients with higher *GJA4* expression level had shorter PFI and disease-specific survival (DSS) (Figure 4F) (P < 0.05). Finally, an IHC H-score based on our own samples showed that GJA4 was expressed at significantly higher levels in CRC tissues than in paracancerous tissues (Figure 4G and H) (P < 0.05).

Single-Cell Level Analysis of *GJA4*

Herein, we attempted to localize *GJA4* at the single cell level to investigate its potential function. We observed that in normal intestinal epithelium, *GJA4* was predominantly expressed on enteroendocrine cells (Figure 5A). It is interesting to note that in CRC tissues, we observed that *GJA4* was predominantly expressed on fibroblasts but not on CRC cells, like *GJA1*, an oncogene acting as an acid transmitter previously shown to be expressed on fibroblasts (Figure 5B). The results of the TIMER web tool also showed that the expression levels of *GJA1* and *GJA4* were highly positively correlated with the abundance of fibroblasts (Figure 5C and D). We then included an independent sample for validation and found that *GJA4* was consistent with the expression of fibroblast markers such as *FAP, PDPN, COL1A2, DCN, COL3A1, COL6A1, ACTA2* (Figure 5E–G). The co-expression pattern of *GJA4* and *ACTA2* which was not observed on the normal intestinal epithelium (Figure 5H) was confirmed by the IF staining on the CRC specimen (Figure 5I). These results suggested that in CRC tissues, GJA4 was not expressed in tumor cells, and fibroblasts overexpressed GJA4.
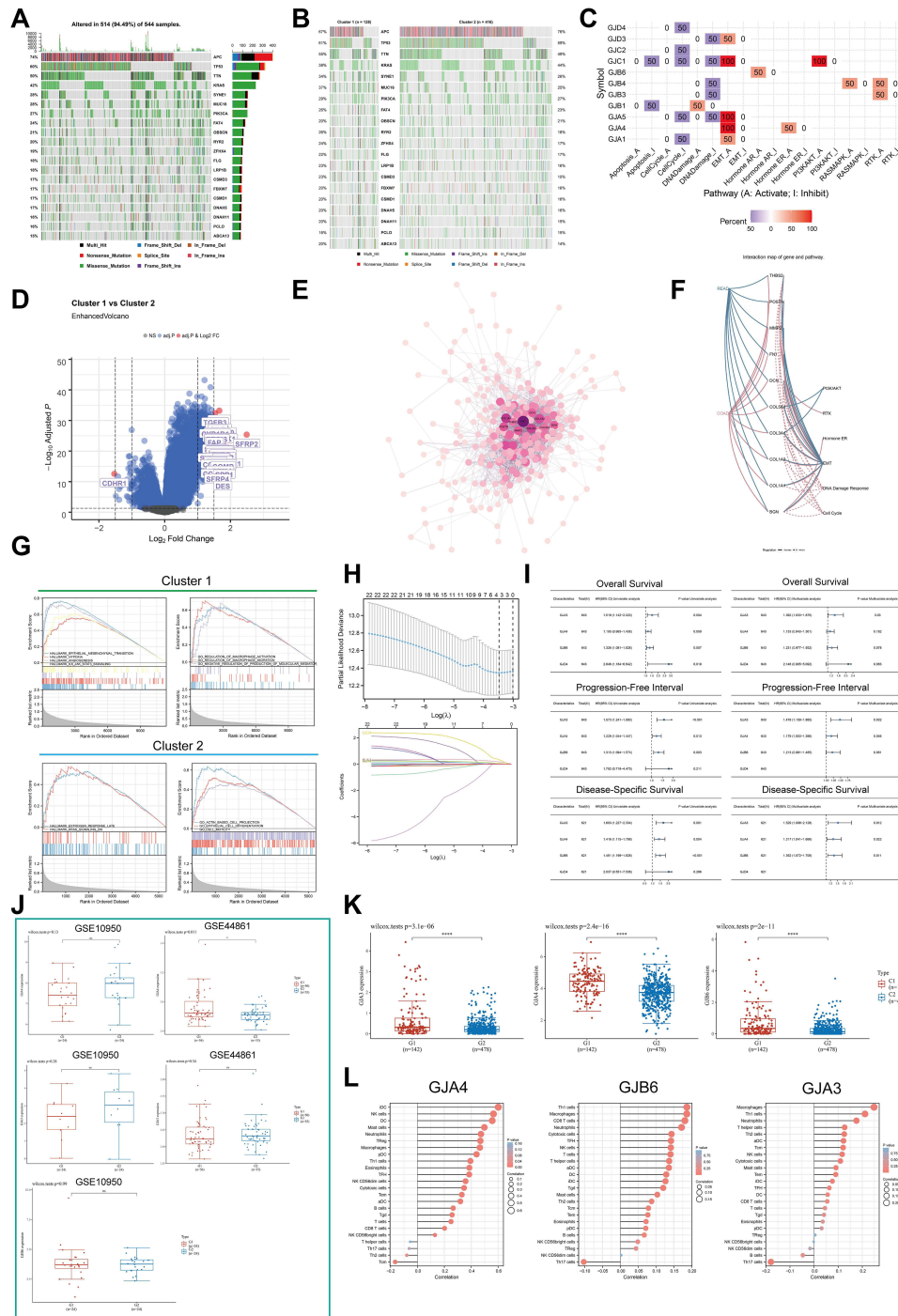
Figure 3 Analysis of connexins-related functions. (**A**) Mutation annotation of the top 20 frequently mutated genes in the TCGA-COADREAD cohort.(**B**) Comparison of the difference in mutation between C1 and C2 clusters. (**C**) The heatmap shows the correlation between the expression level of the 21 connexins in important cancer signaling pathways. The global percentage of cancers in which a gene has an effect on the pathway in COAD and READ, is shown as the percentage: (number of activated/inhibited cancer types/2 *100%). "Pathway activate" (red) represents the percentage of cancers in which a pathway may be activated by given genes, inhibition in a similar way shown as "pathway inhibit" (blue). (**D**) Volcano plot of Differentially expressed genes (DEGs) induced by alterations in connexins levels. red dots, with statistical significance; blue dots, not statistically significant; abscissa, expression differences (log2 fold change); ordinate, significance of differences (−log10 P value). (**E**) Network of DEGs. Darker colors and larger sizes indicate higher degrees. (**F**) The correlation between 10 hub genes from the network and important cancer signaling pathways. Red stands for COAD and blue stands for READ; the solid line represents activation and the dashed line represents inhibition. (**G**) GSEA of the status of special biological pathways in two connexins phenotypes. (**H**) LASSO model fitting. Each curve represents a gene. The profiles of coefficients were plotted versus log(λ). Vertical lines indicate the positions of seven genes with coefficients greater than 0 determined by 10-fold cross-validation. λ was determined from 10-fold cross-validation. The x-axis represents log(λ); the y-axis represents binomial deviance. Optimal values calculated from minimum criteria and one standard error of the criteria are indicated by the dotted vertical lines. (**I**) Univariate Forest plot and multivariate forest plot showing association between 4 candidate genes expression and OS, PFI, DSS in CRC. (**J**) Differential expression of *GJA3, GJA4*, and *GJB6* between normal tissue and CRC tissue by using public datasets from Gene Expression Omnibus (GSE10950 and GSE44861). (**K**) Differential expression of *GJA3, GJA4*, and *GJB6* between C1 and C2 clusters based on TCGA-COADREAD data. (**L**) Relationship between *GJA3, GJA4, GJB6* levels and immune cell infiltration based on ssGSEA. The size of the bubble represents the strength of the correlation and the color of the bubble represents the P-value. (*P < 0.05, ****P < 0.0001).
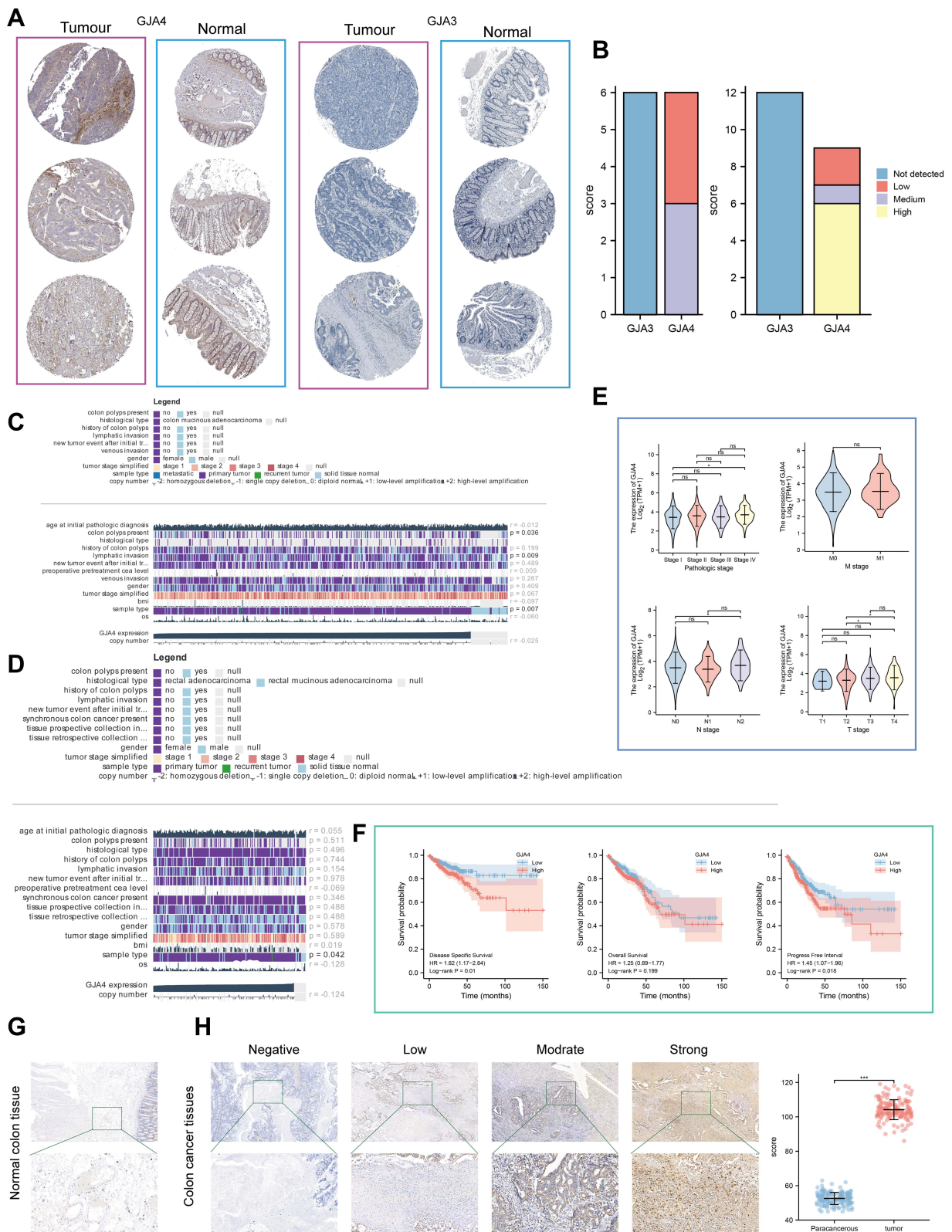**Abbreviation**: NS, not significant.

Figure 4 Clinical value of *GJA4*. (**A**) Representative immunohistochemistry images of GJA4 and GJA3 in CRC and noncancerous tissues derived from the HPA database. (**B**) Staining strengths were annotated as not detected, low, medium, and high. Bar plots indicate the number of samples with different staining strengths. (**C** and **D**) Correlations between *GJA4* level and clinicopathological characteristics in (**C**) COAD and (**D**) READ from MEXPRESS. (**E**) Association of *GJA4* mRNA expression with T/N/M stages and pathological stage in CRC patients. (*P < 0.05). (**F**) OS, DSS, and PFI about *GJA4* based on TCGA-COADREAD. (**G** and **H**) Representative images of different immunohistochemical staining intensities for GJA4 based on our own samples and statistical comparison of GJA4 expression levels (H-SCORE) in (**G**) paracancerous and (**F**) CRC tissue (n = 30). (*P < 0.05, ***P < 0.001).
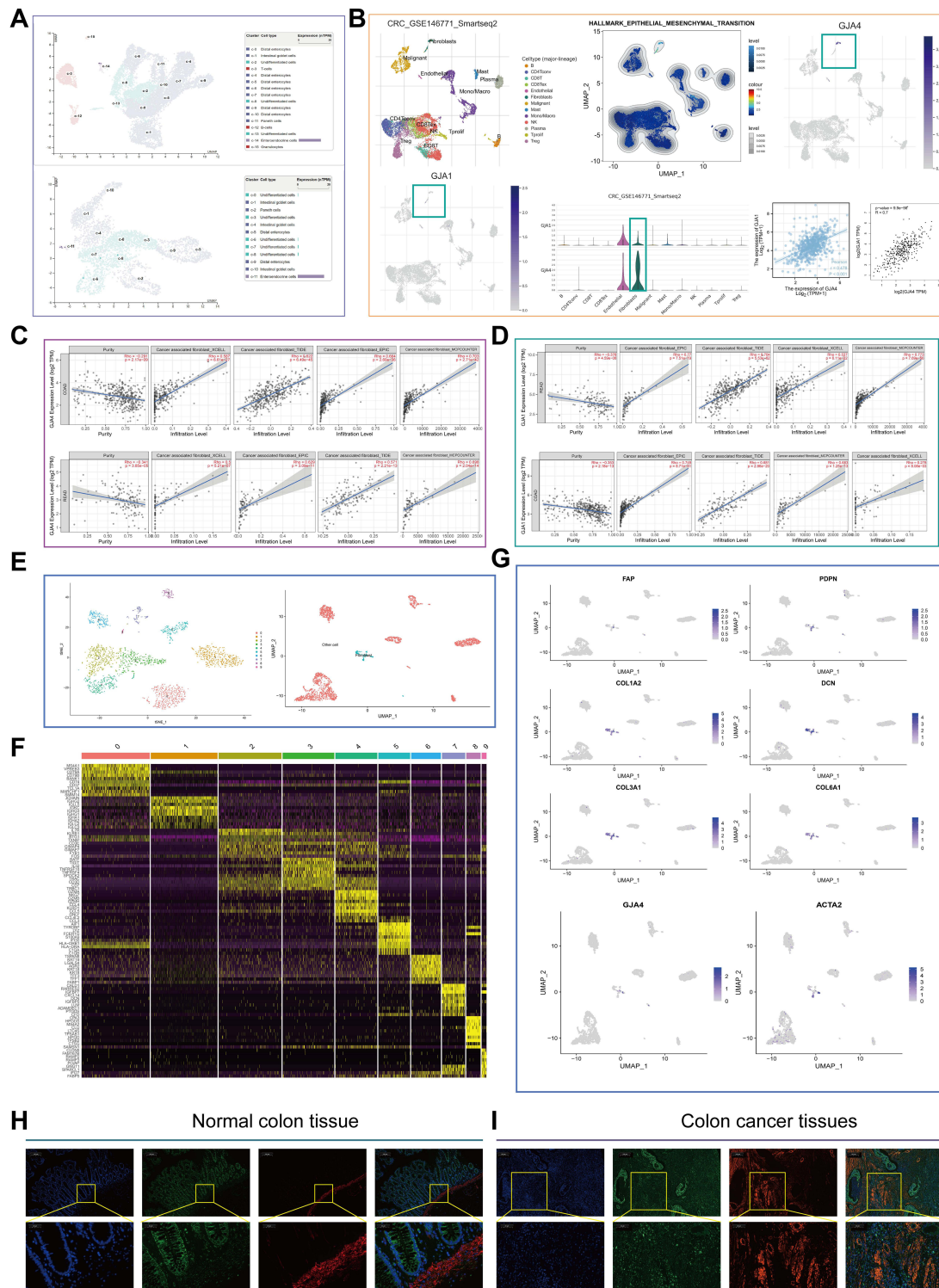**Abbreviation**: NS, not significant.

Figure 5 Single cell analysis and immunofluorescence of GJA4. (**A**) Distribution of *GJA4* in normal intestinal epithelium at single level. (**B**) Single-cell analysis of *GJA4* and *GJA1* based on single cell RNA-seq dataset GSE146771. Uniform Manifold Approximation and Projection (UMAP) plots showing different CRC cell types after quality control, reduction of dimensionality, and clustering; Enrichment scores of genes from the Hallmark EMT signaling gene set for each cell, from gene set variation analysis; UMAP plots showing expression of *GJA4* and *GJA1* clusters; The correlation between *GJA1* and *GJA4* was also calculated based on TCGA-COADREAD and GEPIA, respectively. (**C** and **D**) Dot plot showing the correlation between (**C**) *GJA4*, (**D**) *GJA1* and fibroblasts based on the TIMER web tool. (**E**) Fibroblasts are distinguished from all other cells based on UMAP dimensionality reduction analysis. The t-distributed Stochastic Neighbour Embedding (t-SNE) is also used for dimensionality reduction of the data. (**F**) Heatmap demonstrating each cluster and its gene marker. (**G**) Dot plots demonstrate the expression distribution of *GJA4* and seven fibroblast marker genes. (**H** and **I**) Double immunofluorescence staining images of GJA4 and ACTA2 in the normal and CRC tissue. The representative view of the co-staining of GJA4 and ACTA2 is shown in the enlarged images view below. Scale bars, 100 and 20 mm (enlarged images). Nuclei (DAPI) in blue.

Immune Microenvironment Analysis of *GJA4*

Considering fibroblasts as one of the powerful regulators of the immune microenvironment, we further analyzed the relationship between *GJA4* and immune cells in this section. Through ESTIMATE analysis, we found that *GJA4* was negatively correlated with tumor purity (P < 0.001, R = −0.609; P = 0.002, R = −0.457) and positively correlated with stromal score (P < 0.001, R = 0.536; P = 0.002, R = 0.600; Figure 6A) in the GSE44861 and GSE10950 datasets, respectively. Cellular communication from the scTIME Portal revealed complex interactions among fibroblasts, myeloid cells and malignant cells (Figure 6B). Schematic sketch of intercellular communication in the development of stromal cells is shown in Figure 6C. Fibroblasts have been identified to secrete cytokines to induce macrophages to polarize toward the M2 phenotype to exert inflammatory suppressive effects; therefore, we calculated the correlation between macrophage abundance and the *GJA4* level. We found a positive correlation between the degree of infiltration of M2 macrophages and *GJA4* levels using GSE10950 and GSE44861 (Figure 6D and E), which was then confirmed by IHC staining (Figure 6F). Finally, we searched for genes positively associated with *GJA4* based on its median expression level (Figure 6G) and performed enrichment analysis (Figure 6H), which showed that *GJA4* was closely associated with EMT-related signaling pathways such as "Focal adhesion", "extracellular structure organization", "extracellular matrix organization", and "ECM–receptor interaction".

Discussion

Currently, metastatic colorectal cancer remains the second leading cause of cancer death and places a heavy burden on the health-care system.[41] As a critical step in the process of tumor metastasis, activation of the EMT process is necessary for metastatic growth.[42]

Gap junction is one of the most widely distributed cell junctions and cell-to-cell communication channels in animal tissues, providing a way for the diffusion of low molecular weight substances between cells. In the past few decades, it has been found that it has an inseparable relationship with EMT.[43] There is no doubt that the loss of direct intercellular communication is one of the essential features of cancer cells, a fact that somehow implies the cancer-suppressive properties of gap junctions. Cx43 reduces the growth of rat gliomas in vitro and in vivo,[44] and Cx32 has also been observed to show a reduction in the growth of human liver cancer cells when cells are injected into mice.[45] As research has become more advanced and expanded, there is now a wealth of evidence that connexins are broadly involved in cell proliferation, apoptosis, drug resistance, migration and invasion, but not all studies point to a tumor suppressive effect.[46,47] Interestingly, many of the connexins for which substantial evidence exists as tumor suppressors have been progressively found to be overexpressed and may lead to more aggressive tumor characteristics in some cases. As early as 2000, it was discovered that Cx26 plays a role in tumor cell intra/extravasation by forming heterologous gap junctions with endothelial cells.[48]

Considering such a complex and variable role of connexins, we systematically evaluated the differential expression of 21 connexins-encoding genes at the transcriptome level and found that most of them were overexpressed in tumor tissues compared to normal tissues, in addition, members including *GJA4, GJA5,* and *GJA8* were found to be indicators of poor prognosis. We then classified TCGA-COADREAD cases into two clusters based on the all connexins expression levels by Consensus Clustering, and survival analysis showed that patients in cluster C1 had shorter OS, PFS and DFS than those in cluster C2. Subsequently, we found significant differences in the levels of immune-related factors between the two clusters, and not only that, we also observed that M2 macrophages had higher infiltration levels in cluster C1 relative to cluster C2, whereas macrophage M1, NK cell resting and B cell plasma showed the opposite trend, suggesting that cluster C1 showed a distinct immunosuppressive profile relative to cluster C2. Notably, the sensitivity of tumors to treatment targeting ICPs appears to be governed by the quality and quantity of tumor immune infiltration, and one mechanism by which M2 macrophages promote an immunosuppressive microenvironment appears to be through enhanced expression of ICPs.[49–51] We then calculated that ICPs levels were significantly higher in the cluster C1 than in the cluster C2. In addition, we obtained genes with significantly different expression levels between the two clusters and performed enrichment analysis, which showed that EMT as well as angiogenic phenotypes were significantly activated in the cluster C1, and that most of the hub genes obtained based on the MCC algorithm were also key players in EMT, results that are consistent with the now widely confirmed close association between connexins and EMT. The
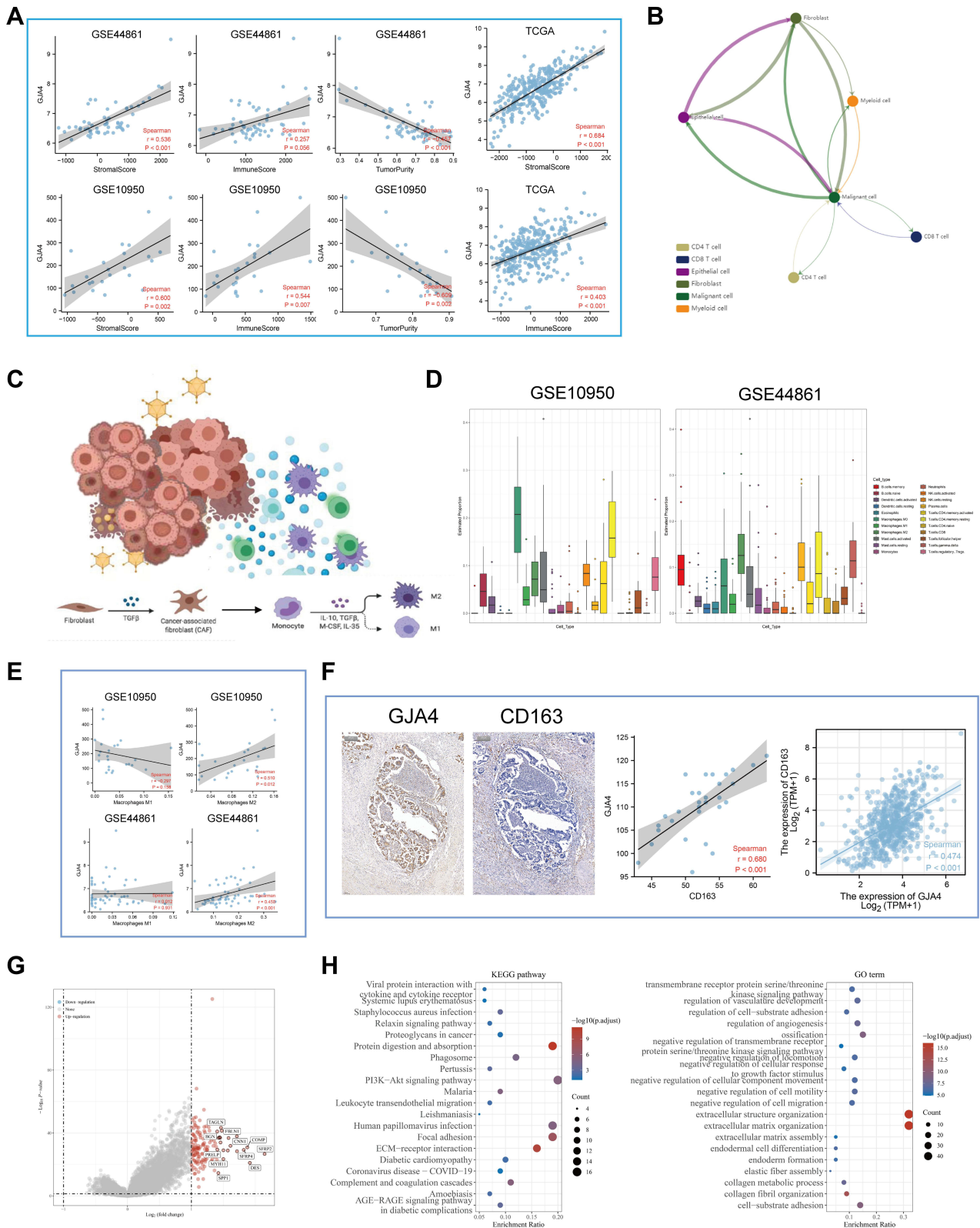
Figure 6 The role of *GJA4* in the immune microenvironment. (**A**) The correlation between GJA4 mRNA expression with stromal/immune score and tumor purity in the GSE44861, GSE10950 and TCGA datasets. (**B**) Cellular communication from scTIME Portal. (**C**) Schematic diagram demonstrating the driving effect of fibroblasts on macrophage polarization. (**D**) Proportion of 22 types of Tumor-initiating cells (TICs) in the CRC tumor samples based on GSE10950 and GSE44861. (**E**) Correlation of the *GJA4* expression levels with macrophage abundance based on GSE10950 and GSE44861. (**F**) Correlation between GJA4 and the M2 macrophage marker CD163 based on immunohistochemical H-score calculation. (**G**) Volcano map showing the genes co-expressed with GJA4. red dots, positively correlated genes; grey dots, not statistically significant; abscissa, expression differences (log2 fold change); ordinate, significance of differences (−log10 P value). (**H**) Functional enrichment analysis of the *GJA4*-related genes including GO and KEGG.

consistent association between EMT-related gene expression and immune cell infiltration suggests an inextricable link between EMT and influencing the response to ICP blockade.

The above results suggested that changes in the expression profile of connexins are closely associated with EMT activation/inhibition. To further identify reliable diagnostic and prognostic indicators, we combined LASSO and COX regression to identify *GJA3, GJA4,* and *GJB6* as independent prognostic factors, and all three were significantly highly expressed in the cluster C1. To determine the sole study target, we further used transcriptomic data from GEO database and immunohistochemical data from HPA database as well as our own patients and found substantial evidence supporting the high expression of GJA4 in tumor tissue. Notably, GJA4 levels correlate with some clinical features of CRC patients, especially high expression in patients with advanced disease. With increasingly refined clinical observations in large samples, there is now a tendency to believe that individual connexins may exhibit dual effects, such as acting as tumor suppressors in primary tumor initiation, but having the opposite effect of promoting cancer progression in advanced disease.

It has been shown that the proliferation of insulinoma cells is significantly slowed upon induced expression of Cx37, a result that is associated with a specific conformation of Cx37.[52] In addition, it has also been reported that the Cx37 C1019T polymorphism may contribute to tumor cell growth.[53] In conclusion, like all other connexin members, Cx37 may have a dual role in tumor development. Unlike Cx43, which has been extensively studied, Cx37 has been reported very sparsely in tumors and has hardly even been reported in CRC. We first observed Cx37 expression in normal intestinal epithelial tissue, mainly on endocrine cells, which are a type of intestinal epithelial cells that secrete granule-releasing peptides and amine-like hormones. However, for CRC tissue, Cx37 was found to be abundantly expressed on fibroblasts, a fraction of cells also enriched for EMT-related genes. Alzbeta Hulikova et al found that the intercellular transmission of acid through gap junctions composed of Cx43 involvement was high between fibroblasts but not between CRC cells.[16] Notably, loss of Cx43 expression was associated with a significant reduction in relapse-free and overall survival of CRC patients and was able to negatively regulate the Wnt signaling pathway thereby enhancing CRC cell apoptosis.[54–56] We speculated that this may reveal an interesting fact that the significance of connexins expression in the parenchymal and stromal components of tumors may be completely opposite. Since gap junctions are mainly composed of 2 connexons, each connexon is composed of 6 subunits (connexins) to form functional unit. Our following calculations revealed a strong positive correlation between Cx37 and Cx43, suggesting a co-activation relationship between the two that may be jointly involved in constituting gap junctions. Results based on four algorithms of the TIMER web tool also indicated that both Cx37 and Cx43 expression levels were significantly positively correlated with fibroblasts abundance. The results of immunofluorescence directly showed that Cx37 was barely expressed on fibroblasts in normal intestinal epithelial tissues, whereas it appeared dramatically on fibroblasts in CRC tissues. While gap junction is a lethal factor for CRC cells, the fact that fibroblasts can help tumor cells metabolize potentially toxic amounts of acid through gap junctions to maintain a pH that is favorable for cancer cell proliferation and invasion results in CRC cells not only excreting excess acid but also minimizing apoptosis and energy burden. We suggest that this may be a microcosm of tumor-stromal interactions.

Since the expression of Cx37 was consistent with the abundance of fibroblasts, the most prominent component of the tumor stromal microenvironment, we continued to investigate the function of Cx37 in the tumor microenvironment. We calculated the relationship between GJA4 levels and stromal scores, immune scores based on three independent datasets and observed a significant positive correlation. It is well established that high immune/stromal scores tend to imply low tumor purity, which not only represents unfavorable survival and high metastatic recurrence rates but also correlates with the immune evasion phenotype. Tumor-associated macrophages usually acquire an immunosuppressive state that suppresses antitumor immunity, which can be induced by CAFs secreting cytokines, the best known of which is stromal-derived growth factor-1.[57–59] Further calculations showed that GJA4 was significantly positively correlated with CD163 both at the protein level and at the transcriptome level, suggesting a role of GJA4 in monocyte trans-differentiation toward the M2 phenotype. Complex malignant crosstalk among cancer cells, cafs and M2 macrophages can synergistically promote EMT of tumor cells to enhance stemness and ultimately contribute to tumor metastasis. Enrichment analysis based on GJA4 expression levels also implied that *GJA4* was closely associated with EMT.

Conclusions

Overall, this study provides a new perspective to understand gap junctions. There is a heterogeneity of gap junctions in CRC, and different gap junctions subtypes showed different prognosis and immune infiltration patterns. How connexins function in tumor progression may be closely related to their localization in the complex tumor microenvironment. We preliminarily recognize Cx37 expressed on fibroblasts as a potential tumor promoter and is associated with a state of immunosuppression. The underlying complex molecular mechanisms and the prognostic and diagnostic value of Cx37 still need to be explored and validated in more experiments and clinical trials with large samples.

Data Sharing Statement

We declare that all the data in this article are authentic, valid, and available for use on reasonable request. Dr Yuan-jie Liu can be contacted (387666719@qq.com) regarding the availability of data and materials.

Ethical Statement

The study's protocol was approved by the ethics committee of the Jiangsu Province Hospital of Chinese Medicine, and informed consent was obtained from clinicians and patients (2020NL-107-01).

Author Contributions

All authors made substantial contributions to conception and design, acquisition of data, or analysis and interpretation of data; took part in drafting the article or revising it critically for important intellectual content; agreed to submit to the current journal; gave final approval of the version to be published; and agreed to be accountable for all aspects of the work.

Funding

Disclosure

The authors declare no conflicts of interest.

References

1. Biller LH, Schrag D. Diagnosis and treatment of metastatic colorectal cancer: a review. *JAMA*. 2021;325(7):669–685. doi:10.1001/jama.2021.0106
2. Kanth P, Inadomi JM. Screening and prevention of colorectal cancer. *BMJ*. 2021;374:n1855. doi:10.1136/bmj.n1855
3. Brenner H, Kloor M, Pox CP. Colorectal cancer. *Lancet*. 2014;383(9927):1490–1502. doi:10.1016/S0140-6736(13)61649-9
4. Robinson JR, Newcomb PA, Hardikar S, et al. Stage IV colorectal cancer primary site and patterns of distant metastasis. *Cancer Epidemiol*. 2017;48:92–95. doi:10.1016/j.canep.2017.04.003
5. Jiang Y, Yuan H, Li Z, et al. Global pattern and trends of colorectal cancer survival: a systematic review of population-based registration data. *Cancer Biol Med*. 2021;18:175–186. doi:10.20892/j.issn.2095-3941.2020.0634
6. Piawah S, Venook AP. Targeted therapy for colorectal cancer metastases: a review of current methods of molecularly targeted therapy and the use of tumor biomarkers in the treatment of metastatic colorectal cancer. *Cancer*. 2019;125(23):4139–4147. doi:10.1002/cncr.32163
7. Modest DP, Pant S, Sartore-Bianchi A. Treatment sequencing in metastatic colorectal cancer. *Eur J Cancer*. 2019;109:70–83. doi:10.1016/j.ejca.2018.12.019
8. Linnekamp JF, Wang X, Medema JP, et al. Colorectal cancer heterogeneity and targeted therapy: a case for molecular disease subtypes. *Cancer Res*. 2015;75(2):245–249. doi:10.1158/0008-5472.CAN-14-2240
9. Lieu CH, Corcoran RB, Overman MJ. Integrating biomarkers and targeted therapy into colorectal cancer management. *Am Soc Clin Oncol Educ Book*. 2019;39(39):207–215. doi:10.1200/EDBK_240839
10. Bhullar DS, Barriuso J, Mullamitha S, et al. Biomarker concordance between primary colorectal cancer and its metastases. *EBioMedicine*. 2019;40:363–374. doi:10.1016/j.ebiom.2019.01.050
11. Nielsen MS, Axelsen LN, Sorgen PL et al. Gap junctions. *Compr Physiol*. 2012;2(3):1981–2035.
12. Beyer EC, Berthoud VM. Gap junction gene and protein families: connexins, innexins, and pannexins. *Biochim Biophys Acta Biomembr*. 2018;1860(1):5–8. doi:10.1016/j.bbamem.2017.05.016

13. Mao XY, Li -Q-Q, Gao Y-F, et al. Gap junction as an intercellular glue: emerging roles in cancer EMT and metastasis. *Cancer Lett*. 2016;381 (1):133–137. doi:10.1016/j.canlet.2016.07.037

14. Bonacquisti EE, Nguyen J. Connexin 43 (Cx43) in cancer: implications for therapeutic approaches via gap junctions. *Cancer Lett*. 2019;442:439–444. doi:10.1016/j.canlet.2018.10.043

15. Thiagarajan PS, Sinyuk M, Turaga SM, et al. Cx26 drives self-renewal in triple-negative breast cancer via interaction with NANOG and focal adhesion kinase. *Nat Commun*. 2018;9(1):578. doi:10.1038/s41467-018-02938-1

16. Hulikova A, Black N, Hsia L-T, et al. Stromal uptake and transmission of acid is a pathway for venting cancer cell-generated acid. *Proc Natl Acad Sci USA*. 2016;113(36):E5344–E5353. doi:10.1073/pnas.1610954113

17. Zhao S, Ye Z, Stanton R. Misuse of RPKM or TPM normalization when comparing across samples and sequencing protocols. *Rna*. 2020;26 (8):903–909. doi:10.1261/rna.074922.120

18. Barrett T, Wilhite SE, Ledoux P, et al. NCBI GEO: archive for functional genomics data sets–update. *Nucleic Acids Res*. 2013;41(Database issue): D991–D995. doi:10.1093/nar/gks1193

19. Wang L, Zhu H, Sun W, et al. Low expression of bestrophin-2 is associated with poor prognosis in colon cancer. *Gene*. 2022;813:146117. doi:10.1016/j.gene.2021.146117

20. Ebadfardzadeh J, Kazemi M, Aghazadeh A, et al. Employing bioinformatics analysis to identify hub genes and microRNAs involved in colorectal cancer. *Med Oncol*. 2021;38(9):114. doi:10.1007/s12032-021-01543-5

21. David CC, Jacobs DJ. Principal component analysis: a method for determining the essential dynamics of proteins. *Methods Mol Biol*. 2014;1084:193–226.

22. Hu JY, Wang Y, Tong X-M, et al. When to consider logistic LASSO regression in multivariate analysis? *Eur J Surg Oncol*. 2021;47(8):2206. doi:10.1016/j.ejso.2021.04.011

23. Koch A, Jeschke J, Van Criekinge W, et al. MEXPRESS update 2019. *Nucleic Acids Res*. 2019;47(W1):W561–W565. doi:10.1093/nar/gkz445

24. Colwill K, Gräslund S. A roadmap to generate renewable protein binders to the human proteome. *Nat Methods*. 2011;8(7):551–558. doi:10.1038/nmeth.1607

25. Bruni D, Angell HK, Galon J. The immune contexture and Immunoscore in cancer prognosis and therapeutic efficacy. *Nat Rev Cancer*. 2020;20 (11):662–680. doi:10.1038/s41568-020-0285-7

26. Magaki S, Hojat SA, Wei B, So A, Yong WH. An introduction to the performance of immunohistochemistry. *Methods Mol Biol*. 2019;1897:289–298.

27. Im K, Mareninov S, Diaz M, Yong WH. An introduction to performing immunofluorescence staining. *Methods Mol Biol*. 2019;1897:299–311.

28. Szklarczyk D, Gable AL, Nastou KC, et al. The STRING database in 2021: customizable protein-protein networks, and functional characterization of user-uploaded gene/measurement sets. *Nucleic Acids Res*. 2021;49(D1):D605–d612. doi:10.1093/nar/gkaa1074

29. Doncheva NT, Morris JH, Gorodkin J, et al. Cytoscape StringApp: network analysis and visualization of proteomics data. *J Proteome Res*. 2019;18 (2):623–632. doi:10.1021/acs.jproteome.8b00702

30. Chin CH, Chen S-H, Wu -H-H, et al. cytoHubba: identifying hub objects and sub-networks from complex interactome. *BMC Syst Biol*. 2014;8 Suppl 4(Suppl 4):S11. doi:10.1186/1752-0509-8-S4-S11

31. Reimand J, Isserlin R, Voisin V, et al. Pathway enrichment analysis and visualization of omics data using g: profiler, GSEA, Cytoscape and enrichment Map. *Nat Protoc*. 2019;14(2):482–517. doi:10.1038/s41596-018-0103-9

32. Kovacic B, Rosner M, Schlangen K, et al. DRUGPATH - a novel bioinformatic approach identifies DNA-damage pathway as a regulator of size maintenance in human ESCs and iPSCs. *Sci Rep*. 2019;9(1):1897. doi:10.1038/s41598-018-37491-w

33. Cao Y, Jiao N, Sun T, et al. CXCL11 correlates with antitumor immunity and an improved prognosis in colon cancer. *Front Cell Dev Biol*. 2021;9:646252. doi:10.3389/fcell.2021.646252

34. Huang Z, Pan J, Wang H, et al. Prognostic significance and tumor immune microenvironment heterogenicity of m5C RNA methylation regulators in triple-negative breast cancer. *Front Cell Dev Biol*. 2021;9:657547. doi:10.3389/fcell.2021.657547

35. Hwang H, Cho G, Jung K, et al. An approach to structural equation modeling with both factors and components: integrated generalized structured component analysis. *Psychol Methods*. 2021;26(3):273–294. doi:10.1037/met0000336

36. Chen B, Khodadoust MS, Liu CL, Newman AM, Alizadeh AA. Profiling tumor infiltrating immune cells with CIBERSORT. *Methods Mol Biol*. 2018;1711:243–259.

37. Chong W, Shang L, Liu J, et al. m 6 A regulator-based methylation modification patterns characterized by distinct tumor microenvironment immune profiles in colon cancer. *Theranostics*. 2021;11(5):2201–2217. doi:10.7150/thno.52717

38. Pan JH, Zhou H, Cooper L, et al. LAYN is a prognostic biomarker and correlated with immune infiltrates in gastric and colon cancers. *Front Immunol*. 2019;10:6. doi:10.3389/fimmu.2019.00006

39. Ma M, Dai J, Tang H, et al. MicroRNA-23a-3p inhibits mucosal melanoma growth and progression through targeting adenylate cyclase 1 and attenuating cAMP and MAPK pathways. *Theranostics*. 2019;9(4):945–960. doi:10.7150/thno.30516

40. Kawamura N, Takaoka K, Hamada H, et al. Rab7-mediated endocytosis establishes patterning of Wnt activity through inactivation of Dkk antagonism. *Cell Rep*. 2020;31(10):107733. doi:10.1016/j.celrep.2020.107733

41. Dekker E, Tanis PJ, Vleugels JLA, et al. Colorectal cancer. *Lancet*. 2019;394(10207):1467–1480. doi:10.1016/S0140-6736(19)32319-0

42. Hu JL, Wang W, Lan XL, et al. CAFs secreted exosomes promote metastasis and chemotherapy resistance by enhancing cell stemness and epithelial-mesenchymal transition in colorectal cancer. *Mol Cancer*. 2019;18(1):91. doi:10.1186/s12943-019-1019-x

43. Yang J, Qin G, Luo M, et al. Reciprocal positive regulation between Cx26 and PI3K/Akt pathway confers acquired gefitinib resistance in NSCLC cells via GJIC-independent induction of EMT. *Cell Death Dis*. 2015;6(7):e1829. doi:10.1038/cddis.2015.197

44. Naus CC, Aftab Q, Sin WC. Common mechanisms linking connexin43 to neural progenitor cell migration and glioma invasion. *Semin Cell Dev Biol*. 2016;50:59–66. doi:10.1016/j.semcdb.2015.12.008

45. Xiang Y, Wang Q, Guo Y, et al. Cx32 exerts anti-apoptotic and pro-tumor effects via the epidermal growth factor receptor pathway in hepatocellular carcinoma. *J Exp Clin Cancer Res*. 2019;38(1):145. doi:10.1186/s13046-019-1142-y

46. Kotini M, Mayor R. Connexins in migration during development and cancer. *Dev Biol*. 2015;401(1):143–151. doi:10.1016/j.ydbio.2014.12.023

47. Czyż J, Szpak K, Madeja Z. The role of connexins in prostate cancer promotion and progression. *Nat Rev Urol*. 2012;9(5):274–282. doi:10.1038/nrurol.2012.14

48. Zeng SG, Lin X, Liu J-C, et al. Hypoxia-induced internalization of connexin 26 and connexin 43 in pulmonary epithelial cells is involved in the occurrence of non-small cell lung cancer via the P53/MDM2 signaling pathway. *Int J Oncol*. 2019;55(4):845–859. doi:10.3892/ijo.2019.4867

49. Narayanapillai SC, Han YH, Song JM, et al. Modulation of the PD-1/PD-L1 immune checkpoint axis during inflammation-associated lung tumorigenesis. *Carcinogenesis*. 2020;41(11):1518–1528. doi:10.1093/carcin/bgaa059

50. Borcoman E, De La Rochere P, Richer W, et al. Inhibition of PI3K pathway increases immune infiltrate in muscle-invasive bladder cancer. *Oncoimmunology*. 2019;8(5):e1581556. doi:10.1080/2162402X.2019.1581556

51. Gong Z, Zhang J, Guo W. Tumor purity as a prognosis and immunotherapy relevant feature in gastric cancer. *Cancer Med*. 2020;9(23):9052–9063. doi:10.1002/cam4.3505

52. Nelson TK, Sorgen PL, Burt JM. Carboxy terminus and pore-forming domain properties specific to Cx37 are necessary for Cx37-mediated suppression of insulinoma cell proliferation. *Am J Physiol Cell Physiol*. 2013;305(12):C1246–C1256. doi:10.1152/ajpcell.00159.2013

53. Morel S, Burnier L, Roatti A, et al. Unexpected role for the human Cx37 C1019T polymorphism in tumour cell proliferation. *Carcinogenesis*. 2010;31(11):1922–1931. doi:10.1093/carcin/bgq170

54. Su YJ, Zhang J-X, Li S-M, et al. Relationship of vasculogenic mimicry, SphK1 expression, and Cx43 expression to metastasis and prognosis in colorectal cancer. *Int J Clin Exp Pathol*. 2018;11(11):5290–5299.

55. Gupta A, Chatree S, Buo AM, et al. Connexin43 enhances Wnt and PGE2-dependent activation of β-catenin in osteoblasts. *Pflugers Arch*. 2019;471 (9):1235–1243. doi:10.1007/s00424-019-02295-y

56. Fostok S, El-Sibai M, Bazzoun D, et al. Connexin 43 loss triggers cell cycle entry and invasion in non-neoplastic breast epithelium: a role for noncanonical Wnt signaling. *Cancers*. 2019;11(3):339. doi:10.3390/cancers11030339

57. Loeuillard E, Yang J, Buckarma E, et al. Targeting tumor-associated macrophages and granulocytic myeloid-derived suppressor cells augments PD-1 blockade in cholangiocarcinoma. *J Clin Invest*. 2020;130(10):5380–5396. doi:10.1172/JCI137110

58. Bu L, Baba H, Yoshida N, et al. Biological heterogeneity and versatility of cancer-associated fibroblasts in the tumor microenvironment. *Oncogene*. 2019;38(25):4887–4901. doi:10.1038/s41388-019-0765-y

59. Zhang R, Qi F, Zhao F, et al. Cancer-associated fibroblasts enhance tumor-associated macrophages enrichment and suppress NK cells function in colorectal cancer. *Cell Death Dis*. 2019;10(4):273. doi:10.1038/s41419-019-1435-2